Energy exchange between Nd^{3+} and Er^{3+} centers within molecular complexes

Diamantoula Maniaki,[a,b] Annika Sickinger,[d] Leoní A. Barrios,[a,b] David Aguilà,[a,b] Olivier Roubeau,[e] Yannick Guyot,[f] François Riobé,[d,g] Olivier Maury,[d] Laura Abad Galán,[c,*] and Guillem Aromí [a,b,*]

[a.] *Departament de Química Inorgànica i Orgànica, Universitat de Barcelona, Diagonal 645, 08028 Barcelona, Spain. E-mail: aromi@ub.edu.*
[b.] *Institute of Nanoscience and Nanotechnology of the University of Barcelona (IN2UB), Barcelona, Spain.*
[c.] *Departamento de Química Inorgánica, Universidad Complutense de Madrid, Avda. Complutense s/n 28040 Madrid, Spain. E-mail: E-mail: laabad03@ucm.es*
[d.] *Univ Lyon, ENS Lyon, CNRS, UMR 5182, Laboratoire de Chimie, F69342 Lyon, France.*
[e.] *Instituto de Nanociencia y Materiales de Aragón (INMA), CSIC and Universidad de Zaragoza, Plaza San Francisco s/n, 50009, Zaragoza, Spain.*
[f.] *Univ. Lyon, Institut Lumière Matière, UMR 5306 CNRS–Université Claude Bernard, Lyon 1, 10 rue Ada Byron, F-69622 Villeurbanne Cedex, France.*
[g.] *Univ. Bordeaux, CNRS, Bordeaux INP, ICMCB UMR 5026, F-33600 Pessac, France.*

Abstract

The controlled and reproducible molecular assemblies incorporating lanthanide centers represents a crucial step in driving forward up- and down-conversion processes. This challenge calls for the development of strategies to facilitate the efficient *in-situ* segregation of different Ln metal ions into distinct positions within the molecule. The unique family of pure [LnLn'Ln] heterometallic coordination compounds previously developed by us represents an ideal platform for studying the desired Ln-to-Ln' energy transfer (ET). In this context, we report here the new pure one-step synthetically produced [ErNdEr] (**3**) complex, which allows for the first time at the molecular level to study the mechanisms behind Nd-to-Er energy transfer. To further assess the photophysical properties of this complex, the analogous [LuNdLu] (**1**) and [ErLaEr] (**2**) complexes have been also prepared and photophysically studied. Efficient sensitization via the two β-diketones employed as main ligands was proben for both Nd^{3+} and Er^{3+} ions, resulting in highly resolved emission spectra and sufficiently long excited state lifetimes, which allowed to further assess the Ln-to-Ln' ET. This intermetallic transfer was first detected by comparing the emission spectra of iso-absorbant solutions and demonstrated by comparing the lifetime values with or without the lanthanide quencher (Er^{3+}), as well as with a deep analysis of the excitation spectrum of the three complexes. Thus, a very unique phenomenon was discovered, consisting in a mutual Nd-to-Er and Er-to-Nd ET with no net increase of brightness by any metal ; while Nd^{3+} transfers the energy received from the antena to Er^{3+}, the sensitization of the latter results into back-transfer to Nd^{3+} to a non-emissive, thus silent state.

Introduction

Lanthanides in their trivalent form (Ln^{3+}) are well known for their characteristic optical (and also magnetic) properties. The specific electronic configuration $4f^n5s^25p^6$ (n= 0-14) when zero-valent, in which the 4f inner shell is well shielded by the 5s and 5p orbitals, gives rise to long-lived excited states with sharp 4f emission bands that span from the near-infrared (NIR) to the visible and UV regions. These optimal photoluminescence properties account for their application in medical imaging,[1-3] telecommunications,[4-6] light emitting devices[7] and solar energy harvesting[8-10] among other areas.[11] Ln ions have the major drawback that their intraconfigurational f-f electronic transitions are mostly forbidden by the selection rules, resulting in very low absorption coefficients. This can be overcome by the presence of a light-harvesting antenna which efficiently transfers the absorbed energy to the lanthanide ions, bringing them into excited states. Conjugated organic groups[12, 13] and charge transfer states of d-metal complexes,[14-16] are often presented as the most efficient vectors of lanthanide sensitization. In addition, the electronic configuration of the Ln atoms leads to the presence of ($\frac{\mathbf{14!}}{\boldsymbol{n!\times(14-n)!}}$) electronic levels and ladder-like energy diagrams with, thus, setting up a perfect platform of possible lanthanide to lanthanide (Ln-to-Ln', Ln ≠ Ln') energy transfer events resulting in up- and down-conversion processes.[17] While these processes have been extensively studied on solids[18-20] and more recently on nanoparticles,[21-24] there is a growing interest in exploring their potential at the molecular scale, using stable, well defined and reproducible molecular assemblies.[25] Regarding up-conversion processes, improvements have been recently obtained with complexes presenting mainly the following pairs: Tb/Yb,[26, 27] Eu/Yb[28] and Yb/Er.[29-31] This anti-Stokes luminescence process (lower-to-higher energy transfer) bears significant potential for various applications that require or utilize NIR radiation, including deep-tissue imaging, cancer therapy, nano-thermometry, biosensing, display technologies, and solar cells.[21, 32-34] By contrast, down-conversion (higher-to-lower energy transfer) remains less investigated with the majority of the processes studied in solution.[35]

Probing Ln-to-Ln' energy transfer (ET) within molecules is challenging because of the necessity engineer well-defined multi-metallic compounds mixing lanthanide ions with seemingly identical coordination chemistry. [36, 37] Therefore, one-step self-assembly reactions involving different lanthanides often result in mixtures of metal distributions within the molecule[38-41] and thus, very tedious sequential methodologies, such as covalent linkage of preformed coordination complexes,[36, 42-45] are typically employed to obtain site-selective heterometallic Ln molecules. The synthetic procedures that are thermodynamically controlled stem from the ability to discriminate between the different metals ionic radii (rLn). Along these lines, we discovered a system capable to coordinate, with remarkable selectivity, two different lanthanide metals by generating two distinct coordination sites, one able to bind the larger ion and the other the smaller one.[46-48] These structures were observed with heteroleptic complexes using multitopic ligands combining ONO chelates (dipicolinate type) with diketonate moieties. This principle has been successfully replicated with a different architecture thus underlining its great potential.[49] The new molecular structure was revealed by mixing two ligands (**Fig. 1**), both with dipicolinate (O,N,O) and diketonate (O,O) units (H_2LA, 2,6-bis[(3-oxo-3-naphthalene-2-yl)-propionyl]pyridine; H_2LB, 6-(3-(naphthalene-2-yl)-3-oxopropanoyl)-picolinic acid), with certain combinations of two different $Ln(NO_3)_3$ salts. As a result, both metals are selectively positioned in a [LnLn'Ln] topology. The selectivity presented by these systems, as well as a distance between centers of ~3.8 Å, allowed us to use this platform to study the intramolecular ET processes. Indeed, we succeeded in studying the Nd-to-Yb ET in the Nd/Yb pair by isolating the [NdYb][50] and [YbNdYb][51] complexes. We noted that in the case of the trinuclear analogue, the existence of two acceptors per donor dramatically enhances the efficiency of this photophysical process. These findings provide noteworthy examples of down conversion processes in heteronuclear complexes, very little studied so far. The down conversion intramolecular energy transfer have only been presented in the visible region with the Tb/Eu,[52-54] and Dy/Tb[43] pairs and, more interestingly, in the NIR region with the Eu/Nd,[55] Nd/Yb,[50, 51, 56, 57] Tb/Yb[58] and Yb/Er.[52, 59-61]

This work presents, to our knowledge, the first case of direct energy transfer between Nd^{3+} and Er^{3+} centers in molecular complexes, specifically, on pure heterometallic molecules. This transfer was first observed in glasses in the 1990s,[62, 63] but had not been studied further in molecular systems. Hereby, we synthesized and determined the structure of a new compound, $[Er_2Nd(LA)_2(LB)2(H_2O)_2(py)](NO_3)$, here termed also [ErNdEr] (**3**), which effectively promotes intramolecular ET from Er to Nd. The photophysical properties of this complex, as well as those of the previously reported $[Lu_2Nd(LA)_2(LB)_2(H_2O)_2(py)](NO_3)$[51] or [LuNdLu] (**1**) and $[Er_2La(LA)_2(LB)_2(H2O)_2(py)](NO_3)$[64] or [ErLaEr] (**2**) were thoroughly investigated to best characterize the desired Nd-to-Er ET.

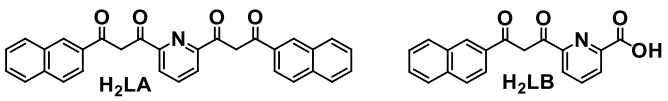

Figure 1. Ligands 1,3-bis-(3-oxo-3-naphthalene-2-yl)propionyl)-pyridine (H_2LA) and 6-(3-(naphthalene-2-yl)-3-oxopropanoyl)-picolinic acid (H_2LB).

Results and discussion

Synthesis. The new complex $[Er_2Nd(LA)_2(LB)_2(H_2O)_2(py)](NO_3)$ (**3**), which allowed to unveil the phenomenon reported here, was obtained as single crystals from a one-step reaction between the stoichiometric amounts of $Er(NO_3)_3$, $Nd(NO_3)_3$, H_2LA and H_2LB in pyridine, following the diffusion of heptane. The chemical process is amenable to a description with a balanced chemical equation that invokes the presence of adventitious water (Eq. 1):

$$2Er(NO_3)_3 + Nd(NO_3)_3 + 2H_2LA + 2H_2LB + 2H_2O + 9py \rightarrow$$
$$\rightarrow [Er_2Nd(LA)_2(LB)_2(H_2O)_2(py)](NO_3) + 8HpyNO_3 \quad (1)$$

Formation of suitable single crystals of **3** required the addition of one equivalent of $CuCl_2$, which does not participate of the reaction but presumably plays a role of modulator of the crystallization (see SI for details).[65] The formulation of **3** was established by single-crystal X-ray diffraction (SCXRD, see below). The uniqueness of this compound is its strict and well defined heterometallic nature, exhibiting two Er^{3+} atoms per atom of Nd^{3+}. Indeed, multinuclear Ln complexes from one step reactions frequently feature quasi-statistical distributions of the different metal types within the molecule, since they have very similar chemical behavior.[38] In the present case, the scaffold generated by LA^{2-} and LB^{2-} generates coordination sites of two distinct types (the central and the peripheral ones) that favor longer metal-to-donor bond distances in the central location, driving the binding of the larger metal to this position (see structural details below). The purity of the bulk material is supported by C, H, N microanalysis and inductively coupled plasma (ICP) metal content determinations, the latter providing a molar Nd/Er ratio of 0.53. The formulation was also consistent with the response from variable temperature molar paramagnetic susceptibility and variable field magnetization measurements (details in SI and **Fig. S1**), which are ascribed to the presence of one Nd^{3+} and two Er^{3+} ions within a molecule with the molecular mass of **3**. The persistence of the architecture of complex **3** in solution was established by mass spectrometry (MS), which unveiled several signals from the trinuclear complex containing its four bridging ligands (Figs. S2 to S4). The absence of any trinuclear moiety with a metal composition other than [ErNdEr] reveals that no metal scrambling occurs.

Structure. Detailed information on the molecular structure of **3** was obtained from SCXRD data collected at 100 K. Its crystal lattice belongs to the triclinic space group $P\overline{1}$. The asymmetric unit is made of one formula unit of **3** and 10 molecules of pyridine. The main [ErNdEr] complex (**Fig. 2**) features a quasi-linear trimetallic Er···Nd···Er array (angle of 174.17°) with the metals bridged together by 2 μ_3–LA^{2-} and two μ–LB^{2-} ligands that chelate them with two types of pockets, *bis*-β-diketonates (O,O) and dipicolinate-like sites (O,N,O). The intramolecular Er···Nd separations are 3.944 and 3.947 Å, while the Er···Er distance within the complex is 7.881 Å. Interestingly, the shortest Er···Er intermolecular separation is smaller (6.059 Å, **Fig. S5**).

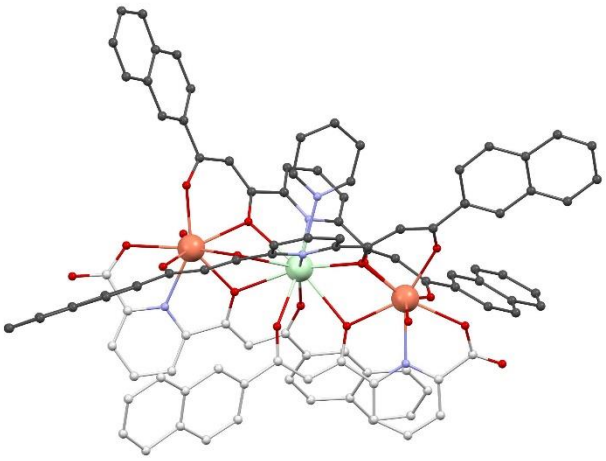

Figure 2. Representation of the cation $[Er_2Nd(LA)_2(LB)_2(H_2O)_2(py)]^+$ of **3** (also representing these of **1** and **2**). The carbon atoms of ligands LA^{2-} and LB^{2-} are darker and lighter gray, respectively). Er is orange, Nd is green, O is red, N is purple and C is gray. H atoms are not shown.

The coordination environment of each Er^{3+} ion is made up of one (O,N,O) and two (O,O) coordination pockets in addition to one molecule of H_2O, thus featuring a coordination number (CN) of 8. The Nd^{3+} centers exhibit two (O,O) and two (O,N,O) chelates and one pyridine ligand, yielding CN 11. The program SHAPE[66] was used to determine the ideal polyhedron that represents best the coordination geometry around each metal. For Er^{3+} it is a biaugmented trigonal prism with normalized distances (in a 0 to 100 scale) of 1.639 (Er1) and 1.487 (Er2). Nd is best represented by capped pentagonal antiprism, calculated to be 6.267 apart from it. The bond distances to the metals were compared using the Ln–O average distances at each center. These average values are 2.32/2.30 and 2.60 Å for Er1/Er2 and Nd, respectively. Thus, the bond distances to the central metal are about 15% longer than to the peripheral metals.

Photophysical Properties. To assist the investigation of the intermolecular Nd-to-Er energy transfer within the [ErNdEr] (**3**) molecule, the analogous [LuNdLu] (**1**) and [ErLaEr] (**2**) complexes were also studied under the same conditions. The experiments were performed on diluted solutions (10^{-4} M) of MeOH-d_4 and DMSO-d_6 (1:1) to avoid intermolecular transfers both at room temperature and at 77 K. Studies in the solid state were also performed to ascertain that the complexes in solution coincide with these described by SCXRD (see below). The main photophysical data extracted from this study are compiled in **Table 1**.

Table 1. Summary of the main photophysical data of complexes **1**, **2** and **3** in a mixture of deuterated MeOH:DMSO (1:1) at room temperature and 77K (between brackets).

Compound	λ_{em} (nm)	τ_{obs} (µs)	Φ_{ET}[b]
LuNdLu (1)	1056	3.99 (3.70)	-
ErLaEr (2)	1550	2.85 (3.50)[a]	-
ErNdEr (3)	1056	1.00 (1.80)	0.75 (0.51)
	1550	1.90 (2.30)[a]	0.33 (0.34)

[a] Measured with an external resistance of 1 kΩ.
[b] Following **Eq. 2**

On previous studies, we established the energy of the triplet excited state of ligands H_2LA and H_2LB to be about 18950 cm^{-1} and 19050 cm^{-1}, respectively.[51] Both energies are sufficiently high to sensitize the $^4F_{3/2}$ state of Nd^{3+} centered at, approximately, 11260 cm^{-1} and the $^4I_{11/2}$ or $^4I_{13/2}$ states of Er^{3+} at 10150 cm^{-1} and ~6500 cm^{-1}. Therefore, emissions at 1056 nm and 1550 nm can be expected from compounds **1** and **2**, respectively. These complexes were thus first investigated to confirm the mentioned antenna effect and to study their luminescence properties.

The photophysics of complex **1** were previously studied in non-deuterated solutions,[51] so in this work the measurements were repeated in deuterated conditions to compare its properties with those of complex **3** (**Fig. 3** and **Fig. S7**). As expected, upon excitation in the ligand transition, **1** presents the characteristic Nd^{3+} transitions at ~880 nm, ~1056 nm and ~1330 nm assigned to $^4F_{3/2} \rightarrow {}^4I_J$ (J = 9/2, 11/2, 13/2). In contrast, an increment of the excited state lifetime at room temperature was observed (3.99 µs *vs* 1.8 µs) due to a decrease of the phonon-mediated non-radiative relaxation enhanced by the use of deuterated solvents.[67] The excitation spectrum (λ_{em} = 1056 nm) at 77 K, shows two types of sensitizations of the excited states of Nd^{3+}, the mentioned antenna effect by energy transfer from the triplet states of the ligands (~375 nm) in addition to direct excitation in the f-f transition (properly assigned in **Fig. 3**).

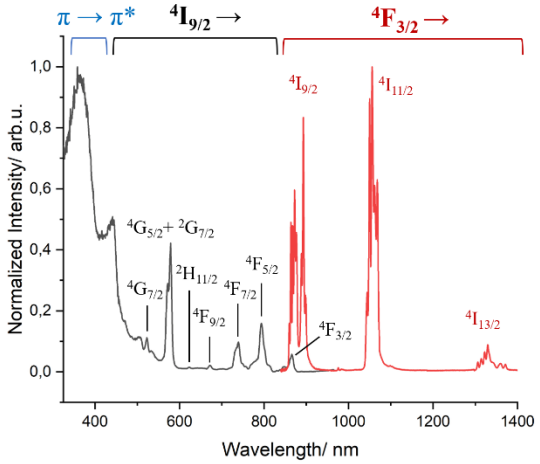

Figure 3. Excitation (λ_{em} = 1056 nm, black trace) and emission (λ_{exc}= 400 nm, red trace) spectra of complex **1** in MeOH-d_4: DMSO-d_6 (1:1) at 77K.

Complex **2** presents the characteristic broad emission band of the $^4I_{13/2} \rightarrow {}^4I_{15/2}$ transition of Er^{3+} centered at 1550 nm. When this spectrum was measured at 77 K, the complicated fine splitting of the $^4I_{15/2}$ state could be observed (**Fig. S8**) in addition of the disappearance of the most "hot bands" of the emissive $^4I_{13/2}$ state.[68] The same fine splitting was observed in frozen solution, indicating that the first coordination environment of Er^{3+} observed in the solid state is kept in solution (**Fig. S7** and **Fig. S8**). The excited-state lifetime decay measured at 1550 nm was fitted with a mono exponential function both at room temperature and 77 K, giving values of 2.85 µs and 3.50 µs, respectively. As seen, lowering the temperature has only a subtle positive effect in the lifetime value by slightly minimizing the non-radiative deactivation. These values are in the typical range of other *β*-diketonate-based Er^{3+} complexes.[69-71] The respective excitation spectra in solution at low temperature show, as for complex **1**, the antenna effect and the direct excitation of the $^4I_{15/2}$ state of Er^{3+}, as depicted in **Fig. 4**.

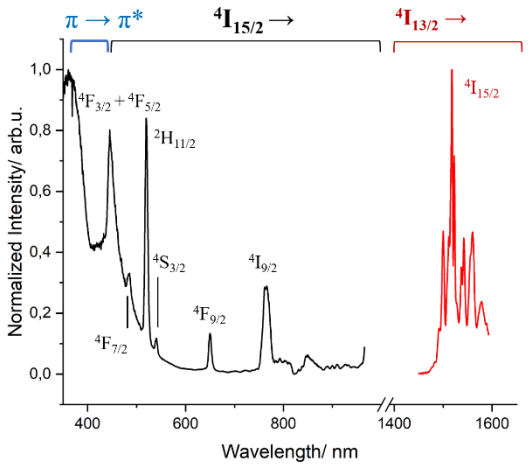

Figure 4. Excitation (λ_{em} = 1550 nm, black trace) and emission (λ_{exc}= 400 nm, red trace) spectra of complex **2** in MeOH-d_4: DMSO-d_6 (1:1) at 77K.

Complex **3** [ErNdEr] was then analyzed to investigate the possible photophysical intercommunication between the two different centers present within the same molecule. The emission spectra upon excitation on the singlet state of the ligands (λ_{exc}= 400 nm), both in solution and the solid state, show luminescence coming from both the $^4F_{3/2}$ state of Nd^{3+} and the $^4I_{13/2}$ one of Er^{3+} (**Fig. S9**). However, this does not allow to confirm the ET between both centers. It only demonstrates an efficient antenna effect occurring when the ligands of the mixed-metal complex are brought to their excited states.

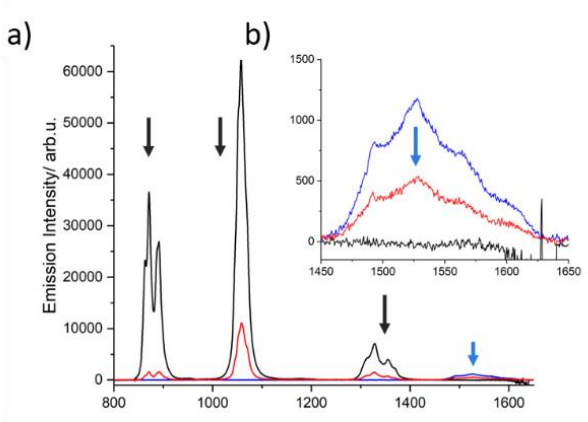

Figure 5. Emission spectra (λ_{exc} = 400 nm) of iso-absorbant solutions of complexes (**1**) (black trace), (**2**) (blue trace), and (**3**) (red trace) in MeOD-d_4: DMSO-d_6 (1:1) solution at room temperature (a) with the correspondent Er^{3+} emission zoom (b).

To further investigate a possible direct ET between both lanthanides, diluted iso-absorbant solutions at 400 nm (OD = 0.4) of complexes **1**, **2** and **3** were compared at room temperature to evaluate changes in intensity of the various characteristic emission bands, in moving from complex to complex. As illustrated in **Fig. 5**, the emission intensity of Nd^{3+} decreases significantly (~80%) from complex **1** to **3**. This pronounced decline cannot be solely attributed to the increase in the number of lanthanide acceptors (one Nd^{3+} in complex **1** *vs.* two Er^{3+} and one Nd^{3+} in complex **3**). The data therefore suggest that another deactivation pathway of Nd^{3+} may be occurring, which we anticipate could be a direct ET to Er^{3+}. This, however, does not correlate with an increase in the Er^{3+} emission in complex **3**, but rather a clear decrease in comparison to complex **2**. The dilution effect is again evident when changing from complex **2** (two Er^{3+}) to **3** (two Er^{3+} and one Nd^{3+}), resulting in an emission decrease of 1/3. Interestingly, the reduction of the Er^{3+} emission (~ 50%) is higher than expected, suggesting that a possible back ET to Nd^{3+} could be also occurring. Similar results were found at 77K. (**Fig S.10**)

This unprecedented hypothesis at molecular level needed further quantitative verification and therefore, the lifetimes of complex **3** were determined in solution at 1056 nm and 1550 nm (**Fig. S11**). The excited state decay at 1056 nm ($^4F_{3/2}$ state of Nd^{3+}) was satisfactorily fitted to a monoexponential function with a lifetime of 1.00 µs at room temperature and 1.80 µs at 77 K. A clear shortening of the lifetime values is observed at both temperatures in comparison with those obtained for the [LuNdLu] (**1**) complex (3.99 µs and 3.70 µs, respectively). Indeed, by using the following equation:

$$\Phi_{ET} = 1 - \frac{\tau_q}{\tau_u} \quad \textbf{(Eq. 2)}$$

the reduction of the lifetime can be translated directly into the efficiency of the energy transfer, amounting to 75% at room temperature and 51% at 77 K. This energy transfer (ET1) is expected to occur from the $^4F_{3/2}$ state of Nd^{3+} to the approximately isoenergetic state/s of Er^{3+}, *i.e.* $^4I_{11/2}$ and/or $^4I_{9/2}$ (**Fig. 6**).[72] The fact that the ET rate was found to be lower at 77K may reflect the fact that at low temperature the transfer $^4F_{3/2} \rightarrow {}^4I_{9/2}$ is not efficient, since latter ($^4I_{9/2}$ of Er^{3+}) lies at higher energy (13089 cm^{-1}) than the $^4F_{3/2}$ state of Nd^{3+} (11338 cm^{-1}), as determined from excitation spectra of "pure" complexes **1** and **2**, respectively (see above). The possibility of the reverse effect, *i.e.* the energy transfer from Er^{3+} to Nd^{3+}, was also investigated. This was conducted by assessing the excited state decay at 1550 nm (that occurring from the state $^4I_{13/2}$ of Er^{3+}) in complex **3**. The mono-exponential fitting of the decay gave lifetime values of 1.90 µs and 2.30 µs at room temperature and 77K, respectively. This suggests an efficient Er^{3+} to Nd^{3+} energy transfer (**Fig. 6**). In this case, this remarkable Er-to-Nd transfer (ET2) occurring from the $^4I_{13/2}$ state of Er^{3+} may be taking place to the $^4I_{15/2}$ or lower lying states of Nd^{3+}.[72, 73] In contrast to the first type of transfer (ET1), ET2 does not result into emission from Nd^{3+} but into non-radiative decay processes, as the ultimate outcome of the partial deactivation of the Er^{3+} emission.

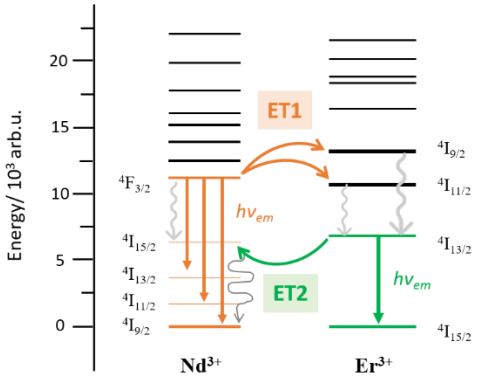

Figure 6. Energy diagram levels of Nd^{3+} and Er^{3+} highlighting the two suggested ET paths occurring within complex **3** [ErNdEr].

Excitation spectra allowed to further characterize this rare intramolecular double ET phenomenon. These were obtained by generating f-f emission transitions within complex **3** in frozen solution. When fixing the detected emission wavelength at 1056 (Nd^{3+} emission), the main excitations lines could be assigned, as expected, to transitions from the $^4I_{9/2}$ state of Nd^{3+}

as for complex **1** (**Fig. 7**). On the other hand, no excitations from Er^{3+} were detected to generate any emission from Nd^{3+}. This observation is not in contradiction with ET2 (Er-to-Nd), as this type of transfer only results in non-radiative deactivation of Er^{3+} instead of any radiative emission (**Fig. 5**). On the other hand, when the emission was fixed at 1550 nm (Er^{3+} emission), two sets of lines could be identified; those from transitions arising from the $^4I_{15/2}$ state of Er^{3+} (also seen in complex **2**) but also, some from exciting the $^4I_{9/2}$ state of Nd^{3+} (**Fig. 7**). This further confirms the direct ET1 (Nd-to-Er) discussed above.

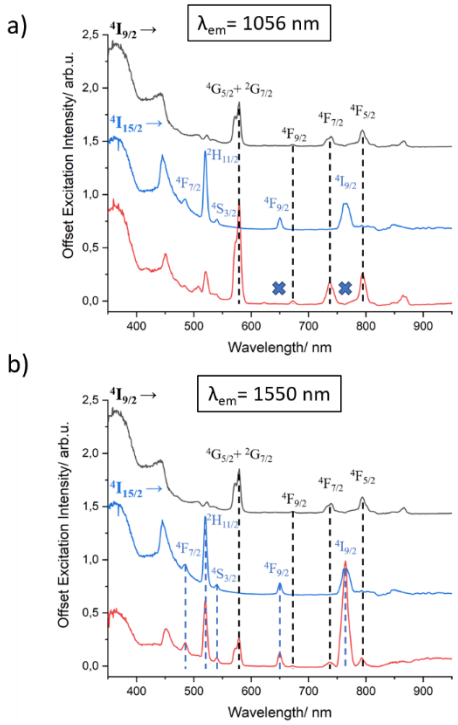

Figure 7. Excitation spectra of complexes (**1**) at λ_{em}= 1056 nm (black trace), (**2**) at λ_{em}= 1550 nm (blue trace) and (**3**, red trace) at λ_{em}= 1056 nm (a) and λ_{em}= 1550 nm (b) in MeOH-d_4/DMSO- d_6 (1:1) at 77 K.

Conclusions

The pure heterometallic [ErNdEr] complex synthesized here allows to unveil the first instance of intramolecular ET between the Nd and Er centers being studied at the molecular level. The ideal distance between both ions (~4 Å) and the specific molecular scaffold have been identified as key parameters in the analysis of the aforementioned transfer. Indeed, the photophysical analysis reveals a rare intramolecular double ET phenomenon. A comparison of the excited state lifetime values in the presence and absence of the lanthanide quencher (Er^{3+} in the case of the Nd-to-Er or Nd^{3+} in the case of Er-to-Nd ET) indicated the presence of two distinct types of transfer. The first one (ET1) occurs from the $^4F_{3/2}$ state of Nd^{3+} to the approximately isoenergetic states of Er^{3+}, *i.e.* $^4I_{11/2}$ and/or $^4I_{9/2}$, which results in the emission of the Er^{3+} $^4I_{11/2}$ state at 1550 nm. In contrast, ET2 occurs from the $^4I_{13/2}$ state of Er^{3+} to the $^4I_{15/2}$ or lower-lying states of Nd^{3+} and does not result in Nd^{3+} emission but in non-radiative decay processes, as the ultimate outcome of the partial deactivation of the Er^{3+} emission. This unprecedented observation was first qualitatively detected by comparing the emission of iso-absorbant solutions and quantitatively confirmed by studying the excited state decays as well as by a critical excitation spectra analysis. The availability of a rich collection of pure heterometallic [LnLn'Ln] complexes offers a great opportunity to discover new intermetallic ET phenomena at the molecular level and their very precise analysis.

Notes and references

1. T. Xian, Q. Meng, F. Gao, M. Hu and X. Wang, *Coord. Chem. Rev.* 2023, **474**, 214866.
2. J.-C. G. Bünzli, *Chem. Rev.* 2010, **110**, 2729-2755.
3. M. C. Heffern, L. M. Matosziuk and T. J. Meade, *Chem. Rev.* 2014, **114**, 4496-4539.
4. J.-C. G. Bünzli and S. V. Eliseeva, *J. Rare Earths* 2010, **28**, 824-842.
5. G. Tessitore, G. A. Mandl, S. L. Maurizio, M. Kaur and J. A. Capobianco, *RSC Adv.* 2023, **13**, 17787-17811.
6. J. H. S. K. Monteiro, *Molecules* 2020, **25**, 2089.
7. S. V. Eliseeva and J.-C. G. Bünzli, *Chem. Soc. Rev.* 2010, **39**, 189-227.
8. J.-C. G. Bünzli and A.-S. Chauvin, in *Handbook on the Physics and Chemistry of Rare Earths*, eds. J.-C. G. Bünzli and V. K. Pecharsky, Elsevier, 2014, vol. 44, pp. 169-281.
9. B. S. Richards, D. Hudry, D. Busko, A. Turshatov and I. A. Howard, *Chem. Rev.* 2021, **121**, 9165-9195.
10. B. M. Van Der Ende, L. Aarts and A. Meijerink, *Phys. Chem. Chem. Phys.* 2009, **11**, 11081.
11. L. E. Mackenzie and R. Pal, *Nature Reviews Chemistry* 2020, **5**, 109-124.
12. J.-C. G. Bünzli and S. V. Eliseeva, Springer Berlin Heidelberg, 2010, DOI: 10.1007/4243_2010_3, pp. 1-45.
13. A. D'Aléo, F. Pointillart, L. Ouahab, C. Andraud and O. Maury, *Coord. Chem. Rev.* 2012, **256**, 1604-1620.
14. S. J. A. Pope, B. J. Coe, S. Faulkner, E. V. Bichenkova, X. Yu and K. T. Douglas, *J. Am. Chem. Soc.* 2004, **126**, 9490-9491.
15. M. D. Ward, *Coord. Chem. Rev.* 2010, **254**, 2634-2642.
16. L.-J. Xu, G.-T. Xu and Z.-N. Chen, *Coord. Chem. Rev.* 2014, **273-274**, 47-62.
17. A. Nadort, J. Zhao and E. M. Goldys, *Nanoscale* 2016, **8**, 13099-13130.
18. S. Zhao, D. Yu, B. Li, S. Kanwal, T. Shen, J. Wu, S. Zhuang and D. Zhang, *Adv. Opt. Mat.* 2024, **12**, 2302408.
19. M. Safdar, A. Ghazy, M. Lastusaari and M. Karppinen, *J. Mater. Chem., C* 2020, **8**, 6946-6965.
20. P. S. David, P. Panigrahi, S. Raman and G. S. Nagarajan, *Mater. Sci. Semicond. Process.* 2021, **122**, 105486.
21. C. Duan, L. Liang, L. Li, R. Zhang and Z. P. Xu, *Journal of Materials Chemistry B* 2018, **6**, 192-209.
22. H. Zhao, Y. Li, X. Zhang, K. Wu, J. Lv, C. Chen, H. Liu, Z. Shi, H. Ju and Y. Liu, *Biomaterials* 2022, **291**, 121873.
23. E. M. Mettenbrink, W. Yang and S. Wilhelm, *Adv. Photonics Res.* 2022, **3**, 2200098.
24. K. Malhotra, D. Hrovat, B. Kumar, G. Qu, J. V. Houten, R. Ahmed, P. A. E. Piunno, P. T. Gunning and U. J. Krull, *ACS Appl. Mater. Interfaces* 2023, **15**, 2499-2528.
25. L. J. Charbonnière, A. M. Nonat, R. C. Knighton and L. Godec, *Chem. Sci.* 2024, **15**, 3048-3059.
26. R. C. Knighton, L. K. Soro, L. Francés-Soriano, A. Rodríguez-Rodríguez, G. Pilet, M. Lenertz, C. Platas-Iglesias, N.

Hildebrandt and L. J. Charbonnière, *Angew. Chem., Int. Ed.* 2022, **61**, e202113114.
27. A. Nonat, S. Bahamyirou, A. Lecointre, F. Przybilla, Y. Mély, C. Platas-Iglesias, F. Camerel, O. Jeannin and L. J. Charbonnière, *J. Am. Chem. Soc.* 2019, **141**, 1568-1576.
28. I. Hernández, N. Pathumakanthar, P. B. Wyatt and W. P. Gillin, *Adv. Mater.* 2010, **22**, 5356-5360.
29. T. V. Balashova, A. P. Pushkarev, A. N. Yablonskiy, B. A. Andreev, I. D. Grishin, R. V. Rumyantcev, G. K. Fukin and M. N. Bochkarev, *J. Lumin.* 2017, **192**, 208-211.
30. J. Wang, Y. Jiang, J.-Y. Liu, H.-B. Xu, Y.-X. Zhang, X. Peng, M. Kurmoo, S. W. Ng and M.-H. Zeng, *Angew. Chem., Int. Ed.* 2021, **60**, 22368-22375.
31. D. A. Gálico, J. S. Ovens, F. A. Sigoli and M. Murugesu, *ACS Nano* 2021, **15**, 5580-5585.
32. S. Goderski, M. Runowski, P. Woźny, V. Lavín and S. Lis, *ACS Applied Materials & Interfaces* 2020, **12**, 40475-40485.
33. A. Gupta, S. Ghosh, M. K. Thakur, J. Zhou, K. Ostrikov, D. Jin and S. Chattopadhyay, *Prog. Mater. Sci.* 2021, **121**, 100838.
34. X. Qin, J. Xu, Y. Wu and X. Liu, *ACS Central Science* 2019, **5**, 29-42.
35. S. Lis, M. Elbanowski, B. Mąkowska and Z. Hnatejko, *J. Photochem. Photobiol. A* 2002, **150**, 233-247.
36. D. J. Lewis, P. B. Glover, M. C. Solomons and Z. Pikramenou, *J. Am. Chem. Soc.* 2011, **133**, 1033-1043.
37. C. Egger, L. Guénée, N. Deorukhkar and C. Piguet, *Dalton Trans.* 2024, **53**, 6050-6062.
38. F. Artizzu, F. Quochi, L. Marchiò, R. F. Correia, M. Saba, A. Serpe, A. Mura, M. L. Mercuri, G. Bongiovanni and P. Deplano, *Chem., Eur. J.* 2015, **21**, 3833-3833.
39. N. André, T. B. Jensen, R. Scopelliti, D. Imbert, M. Elhabiri, G. Hopfgartner, C. Piguet and J.-C. G. Bünzli, *Inorg. Chem.* 2004, **43**, 515-529.
40. S. Floquet, M. Borkovec, G. Bernardinelli, A. Pinto, L.-A. Leuthold, G. Hopfgartner, D. Imbert, J.-C. G. Bünzli and C. Piguet, *Chem., Eur. J.* 2004, **10**, 1091-1105.
41. F. Artizzu, F. Quochi, L. Marchiò, M. Saba, A. Serpe, A. Mura, M. L. Mercuri, G. Bongiovanni and P. Deplano, *MRS Advances* 2016, **1**, 2683-2688.
42. M. P. Placidi, A. J. L. Villaraza, L. S. Natrajan, D. Sykes, A. M. Kenwright and S. Faulkner, *J. Am. Chem. Soc.* 2009, **131**, 9916-9917.
43. T. J. Sørensen, M. Tropiano, O. A. Blackburn, J. A. Tilney, A. M. Kenwright and S. Faulkner, *Chem. Commun.* 2013, **49**, 783-785.
44. J. J. Le Roy, J. Cremers, I. A. Thomlinson, M. Slota, W. K. Myers, P. H. Horton, S. J. Coles, H. L. Anderson and L. Bogani, *Chem. Sci.* 2018, **9**, 8474-8481.
45. C. D. Buch, S. H. Hansen, D. Mitcov, C. M. Tram, G. S. Nichol, E. K. Brechin and S. Piligkos, *Chem. Sci.* 2021, **12**, 6983-6991.
46. D. Aguilà, L. A. Barrios, V. Velasco, O. Roubeau, A. Repollés, P. J. Alonso, J. Sesé, S. J. Teat, F. Luis and G. Aromí, *J. Am. Chem. Soc.* 2014, **136**, 14215-14222.
47. J. Gonzalez-Fabra, N. A. G. Bandeira, V. Velasco, L. A. Barrios, D. Aguila, S. J. Teat, O. Roubeau, C. Bo and G. Aromi, *Chem., Eur. J.* 2017, **23**, 5117-5125.
48. D. Aguila, V. Velasco, L. A. Barrios, J. Gonzalez-Fabra, C. Bo, S. J. Teat, O. Roubeau and G. Aromi, *Inorg. Chem.* 2018, **57**, 8429-8439.
49. V. Velasco, L. A. Barrios, M. Schütze, O. Roubeau, F. Luis, S. J. Teat, D. Aguilà and G. Aromí, *Chem., Eur. J.* 2019, **25**, 15228 – 15232.
50. L. Abad Galán, D. Aguilà, Y. Guyot, V. Velasco, O. Roubeau, S. J. Teat, M. Massi and G. Aromí, *Chem., Eur. J.* 2021, **27**, 7288 –7299.
51. D. Maniaki, A. Sickinger, L. A. Barrios Moreno, D. Aguilà, O. Roubeau, N. S. Settineri, Y. Guyot, F. Riobé, O. Maury, L. A. Galán and G. Aromí, *Inorg. Chem.* 2023, **62**, 3106-3115.
52. H.-B. Xu, J.-G. Deng, L.-Y. Zhang and Z.-N. Chen, *Cryst. Growth Des.* 2013, **13**, 849-857.
53. H. Yao, G. Calvez, C. Daiguebonne, K. Bernot, Y. Suffren, M. Puget, C. Lescop and O. Guillou, *Inorg. Chem.* 2017, **56**, 14632-14642.
54. T. Chuasaard, P. Jittipiboonwat, A. Ngamjarurojana, B. Yotnoi and A. Rujiwatra, *J. Solid State Chem.* 2023, **324**, 124075.
55. L. Abad Galán, A. N. Sobolev, B. W. Skelton, E. Zysman-Colman, M. I. Ogden and M. Massi, *Dalton Trans.* 2018, **47**, 12345-12352.
56. F. Artizzu, A. Serpe, L. Marchiò, M. Saba, A. Mura, M. L. Mercuri, G. Bongiovanni, P. Deplano and F. Quochi, *J. Mater. Chem., C* 2015, **3**, 11524-11530.
57. M. Oggianu, V. Mameli, M. A. Hernández-Rodríguez, N. Monni, M. Souto, C. D. S. Brites, C. Cannas, F. Manna, F. Quochi, E. Cadoni, N. Masciocchi, A. N. Carneiro Neto, L. D. Carlos and M. L. Mercuri, *Chem. Mater.* 2024, **36**, 3452-3463.
58. S. Faulkner and S. J. A. Pope, *J. Am. Chem. Soc.* 2003, **125**, 10526-10527.
59. F. Artizzu, F. Quochi, L. Marchiò, E. Sessini, M. Saba, A. Serpe, A. Mura, M. L. Mercuri, G. Bongiovanni and P. Deplano, *J. Phys. Chem. Lett.* 2013, **4**, 3062-3066.
60. F. Artizzu, F. Quochi, L. Marchiò, C. Figus, D. Loche, M. Atzori, V. Sarritzu, A. M. Kaczmarek, R. Van Deun, M. Saba, A. Serpe, A. Mura, M. L. Mercuri, G. Bongiovanni and P. Deplano, *Chem. Mater.* 2015, **27**, 4082-4092.
61. L. Song, Q. Wang, D. Tang, X. Liu and Z. Zhen, *New J. Chem.* 2007, **31**, 506-511.
62. W. Q. Shi, M. Bass and M. Birnbaum, *J. Opt. Soc. Am. B* 1989, **6**, 23-29.
63. O. Barbosa-García, R. A. McFarlane, M. Birnbaum and L. A. Díaz-Torres, *J. Opt. Soc. Am. B* 1997, **14**, 2731-2734.
64. E. Macaluso, M. Rubín, D. Aguilà, A. Chiesa, L. A. Barrios, J. I. Martínez, P. J. Alonso, O. Roubeau, F. Luis, G. Aromí and S. Carretta, *Chem. Sci.* 2020, **11**, 10337-10343.
65. R. S. Forgan, *Chem. Sci.* 2020, **11**, 4546-4562.
66. P. Alemany, D. Casanova, S. Alvarez, C. Dryzun and D. Avnir, in *Rev. Comput. Chem.*, 2017, DOI: https://doi.org/10.1002/9781119356059.ch7, pp. 289-352.
67. A. d. Bettencourt-Dias, *Luminescence of lanthanide ions in coordination compounds and nanomaterials*, Wiley, Chichester, U.K., 2014.
68. A. Sickinger, B. Baguenard, A. Bensalah-Ledoux, Y. Guyot, L. Guy, F. Pointillart, O. Cador, M. Grasser, B. Le Guennic, F. Riobé, O. Maury and S. Guy, *J. Mater. Chem., C* 2024, **12**, 4253-4260.
69. L. A. Galán, B. L. Reid, S. Stagni, A. N. Sobolev, B. W. Skelton, M. Cocchi, J. M. Malicka, E. Zysman-Colman, E. G. Moore, M. I. Ogden and M. Massi, *Inorg. Chem.* 2017, **56**, 8975-8985.
70. P. Martín-Ramos, I. R. Martín, F. Lahoz, S. Hernández-Navarro, P. S. Pereira da Silva, I. Hernández, V. Lavín and M. Ramos Silva, *J. Alloys Compd.* 2015, **619**, 553-559.

71. Z. Ahmed, R. E. Aderne, J. Kai, J. A. L. C. Resende, H. I. Padilla-Chavarría and M. Cremona, *RSC Adv.* 2017, **7**, 18239-18251.
72. Y. Liu, Y. Sun, Y. Wang, Z. You, Z. Zhu, J. Li and C. Tu, *J. Lumin.* 2018, **198**, 40-45.
73. Y. Wang, J. Li, Z. Zhu, Z. You, J. Xu and C. Tu, *Optics Express* 2015, **23**, 18554.